# STRUCTURAL ACOUSTICS TUTORIAL—PART 2: SOUND—STRUCTURE INTERACTION

**Stephen A. Hambric**

and

**John B. Fahnline**

*Applied Research Laboratory, The Pennsylvania State University*
*State College, Pennsylvania 16804*

## Introduction

This is the second of a two-part tutorial on structural acoustics written for *Acoustics Today*. The first appeared in the October 2006 issue, and focused on vibrations in structures. In that article, I explained

- the various waves that can propagate through structures, and how bending waves are dispersive (their wavespeeds increase with frequency);
- the modes of vibration of finite structures;
- mobility and impedance, and how they are simply summations of individual modal responses;
- structural damping;
- how the mobility of an infinite structure is the mean mobility of a finite one; and
- modeling vibrations with finite element (FE) analysis.

Some of the feedback I received from readers of the first article pointed out that it was more of a 'cliffs notes' summary of structural acoustics than a tutorial, but found the summary quite useful nevertheless. After thinking about it, I suppose that is true, and I thought about renaming the second part of this article 'A Structural Acoustics Cookbook,' rather than a tutorial. For continuity, though, I have retained the original title, but hope the two articles will be a useful short reference on the subject, where handy formulas and concepts can be easily found.

*"In this article we will explain: what structural vibrations do to neighboring acoustic fluids, and what sound fields do to neighboring structures."*

In this article, I have added a co-author—Dr. John Fahnline—who specializes in analyzing sound–structure interaction using boundary element (BE) modeling techniques. John has already written one book[1] on acoustic BE analysis (with Gary Koopmann), and is working on a second.

In this article we will explain:

- what structural vibrations do to neighboring acoustic fluids, and
- what sound fields do to neighboring structures.

These problems are complementary (and reciprocal), and we will use analytic, numerical, and experimental data to demonstrate their basic concepts. As with Part 1 of the article, we will supply plenty of useful terms and equations.

The overarching concept of linear sound–structure interaction is simple: the normal particle velocity in the structure and fluid along the fluid–structure interaction boundary must be the same. This means that when a structure vibrates against a fluid, the component of the vibration normal to the structural surface must be identical to the corresponding particle velocity in the neighboring fluid. This simple equality allows us to couple the equations that define structural and fluid motion at the fluid–structure interface and solve for the total sound–structure behavior. While the normal particle velocity is identical in the structure and fluid, the in-plane, or tangent particle velocity is not. In fact, we allow a 'slip condition' between the structure and fluid, so that a structure can slide along a neighboring fluid without inducing any sound.

Of course, with any simple concept there are inevitably several assumptions. Here are ours:

- homogeneity (the fluid properties are the same everywhere),
- isotropy (the fluid properties are the same no matter what direction the wave propagates), and
- linearity (the fluid properties do not depend on the fluctuating pressure amplitude or phase).

With these simplifying assumptions, it is straightforward to couple the vibrations of structures with those in acoustic fluids. Incidentally, all of the information in Part 1 of this article made the same assumptions, but for the structural materials!

We will start by explaining what a structure's vibrations do to a fluid—they compress and expand it. The spatial pattern of structural vibrations and their frequencies determines how much sound is radiated, and in what directions. It may be helpful to think of the acoustic fluid as an elastic blob surrounding the structure, being pushed and pulled over time by the motion of the structural boundary (in the normal direction only, of course). When the fluid's mass density is comparable to the structure's, the fluid not only absorbs sound, but also mass-loads the structure. We will explain how two important structures—a circular baffled piston, and a flat rectangular flexible finite plate—radiate sound and are fluid-loaded by the impedance of the surrounding acoustic fluid.

Next, we will consider the complementary problem—how acoustic waves induce vibration in a structure. The same physics are at work in this reciprocal problem, as we shall see later. We will conclude by discussing how to make measurements of sound–structure interaction, and how to model it using boundary elements.

**A clarifying note**: in this article we consider sound–structure interaction, not fluid–structure interaction

(FSI). FSI usually refers to how moving fluids interact with solid objects, such as the turbulent flow over a structure. To learn more about FSI, we recommend the references by Blevins[2] and Naudascher and Rockwell.[3]

## Piston vibrating against an acoustic fluid

Perhaps no other structural-acoustic system has been studied more than a circular baffled piston vibrating against an acoustic fluid (see, for example, Fahy,[4] pages 58–60 and 118–121; Pierce,[5] pages 220–225; and Junger and Feit,[6] pages 95–100 and 105–109). We will describe how a piston interacts with a surrounding acoustic fluid, and how the acoustic fluid affects the piston's vibrations. This simple problem allows us to introduce many structural-acoustic quantities of interest.

Let us start by considering a very slowly oscillating piston in a rigid baffle, as shown in Fig. 1. As the piston moves outward, fluid flows from the area of high pressure near the center of the piston to its outer edge, which is nearly at ambient pressure. Conversely, as the piston moves inward, fluid flows toward the center of the piston, where the pressure is less than the ambient pressure. The level of sound radiation is a function of frequency because as the speed of the oscillation of the piston increases, there is less and less time for the pressure to equalize, and eventually the surface vibrations become much more efficient in compressing the adjacent fluid and causing sound radiation. Since the piston's size controls how far the pressure pulses have to travel before they can equalize with the surrounding fluid, it is important in determining when it begins to radiate sound efficiently.

Thus, we can conclude purely from physical arguments that the main parameters which control the acoustic radiation from a vibrating structure are its speed of vibration (or frequency) and its size. It is common in acoustics to nondimensionalize the problem in terms of the quantity $ka$, where $k$ is the acoustic wavenumber and $a$ is the characteristic dimension of the vibrating structure. For a piston source, the transition from an inefficient, low frequency oscillation to an efficient, high frequency oscillation occurs at approximately $ka = 1$, where $a$ is the radius of the piston. At this frequency, the acoustic wavelength is of the same order as the size of the structure.

A source with zero average displacement is an even more inefficient radiator of sound at low frequencies, like an unbaffled piston, i.e., a loudspeaker without a cabinet. When the diaphragm of the speaker moves, the fluid on one side of the speaker is compressed while the fluid on the other side is expanded (see Fig. 1). There is a natural flow of fluid from high pressure to low pressure, and thus the fluid flows around the edges of the speaker. The pressure equalization is very nearly complete because the average displacement of the surface is zero when both sides are taken into account, such that there is very little residual compression of the acoustic medium and sound radiation. As the frequency of vibration increases, the sound radiation also increases because there is not as much time for the fluid to flow around the edges of the speaker before it is compressed. At approximately $ka = 1$, a source with zero average displacement becomes as efficient a radiator of sound as a baffled piston.

Let us consider the pressure field radiated by an oscillating piston at discrete frequencies. We assume the piston's

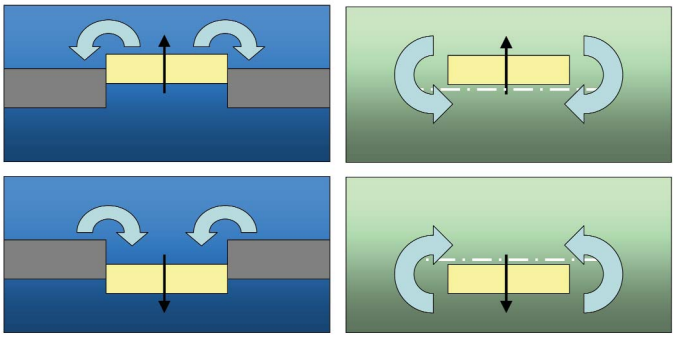

*Fig. 1. Low frequency vibration and acoustic fluid motion of a piston. Left – baffled piston; Right – unbaffled piston.*

vibrations are time harmonic ($e^{i\omega t}$), and consider pressures in the *far-field*, or far away from the structure. The far-field pressure radiated by a baffled circular piston as a function of angle θ and distance $r$ is:

$$p(r,\theta) = i\omega\rho_o a^2 v_n \left[\frac{J_1(k_o a\sin\theta)}{k_o a\sin\theta}\right]\frac{e^{-ik_o r}}{r}, \qquad (1)$$

where $\rho_0$ is the fluid density, $a$ is the piston radius, $v_v$ is the piston velocity (assumed to be constant over the surface of the piston), and $k_o$ is the radial frequency ω divided by the acoustic sound speed $c_o$. We do not include the time-harmonic dependence in this, or in any future equations.

Figure 2 shows the far-field pressure at two frequencies, normalized to $k_o a$, where $k_o a=\pi$ and $3\pi$. For $k_o a=\pi$ (a full acoustic wavelength spanning the piston diameter), the pressure is in phase at all directivity angles (note that the directivity angle is taken from a vector pointing normal to the pis-

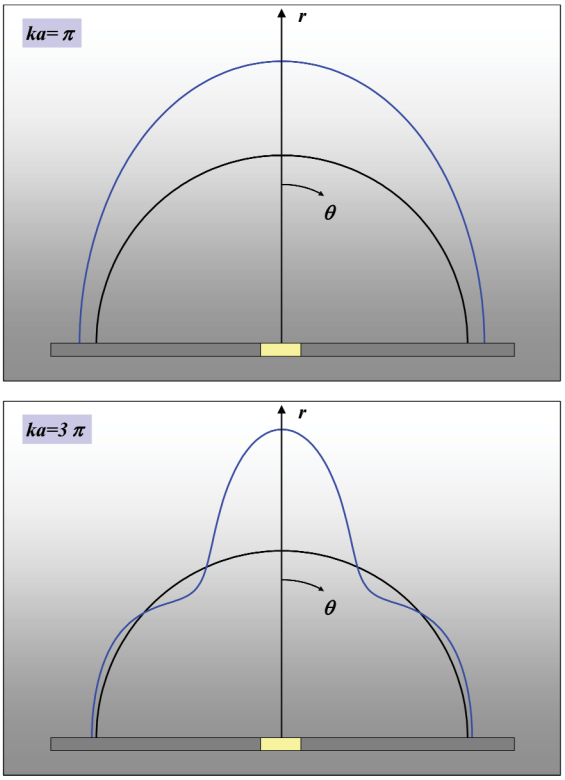


*Fig. 2. Pressure distribution in the far-field of a radiating baffled piston. Top – ka=π; Bottom – ka=3π.*

ton surface). However, at higher frequencies, like $k_o a=3\pi$, the pressure alternates its phase at varying angles. The directivity of the sound radiated by piston sources is usually plotted as a pressure magnitude to remove the effects of alternating phase.

It is hard to generalize how much sound a source makes by considering pressure at a specific location. Therefore, we usually measure or compute the total radiated sound power instead. The total radiated sound power is computed by integrating the active acoustic intensity over space.

The active, or propagating acoustic intensity in a fluctuating acoustic pressure field is:

$$\vec{I} = \frac{1}{2}\mathrm{Re}(p\vec{v}^*) \tag{2}$$

where $\vec{v}^*$ is the conjugate of the acoustic fluctuating particle velocity. Notice that both the particle velocity and intensity are vector quantities, and point in specific directions. When in the far-field, we consider only the radially propagating component of intensity. Also when in the far-field, the pressure and particle velocity are in phase with each other (this is *not* the case close to the vibrating surface, or in the near-field) and $v=p/\rho_o c_o$. So, in the far-field, the radial component of intensity simplifies to:

$$I_{radial} = \frac{1}{2}\frac{|p|^2}{\rho_o c_o} \tag{3}$$

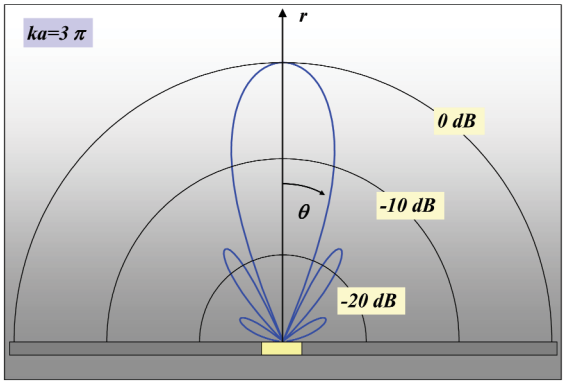


*Fig. 3. Sound intensity distribution in the far-field of a radiating baffled piston, $ka=3\pi$.*

Figure 3 shows the far-field intensity for $ka=3\pi$ on a dB scale. Notice how all the peak locations are positive, since intensity squares the pressure magnitude. The highest pressure is normal to the piston, with lower amplitude side lobes at various angles. As *ka* increases, more side lobes will appear.

The total radiated power is computed by integrating the intensity (which is just the localized power/area) over a far-field half-spherical surface surrounding the piston. Spherical surfaces are used to make the integration simple; the total sound power may be integrated over any shaped surface, though.

The radiated sound power is related directly to the *radiation resistance* of the fluid, which acts over the surface of the

piston. In fact, power can be calculated knowing a structure's radiation resistance and spatially- and time-averaged normal velocity:

$$P_{rad} = R_o \left\langle |v|^2 \right\rangle . \tag{4}$$

The radiation resistance and reactance are the real and imaginary parts of the fluid loading on the structure's surface. Imagine once again the fluid as an encompassing elastic blob surrounding the structure. As the structure pushes against this blob, it encounters an impedance, which resists the structure's motion. The impedance, $Z_o$, is complex, and equal to $R_o + iX_o$, where $X_o$ is the reactance. The resistance and reactance are fluid-loading properties of the structure, and *do not depend on how the structure vibrates*. Equations for the resistance and reactance (shown without derivation) of a baffled circular piston are:

$$R_o = \rho_o c_o A\left(1 - \frac{2J_1(2k_o a)}{2k_o a}\right), \text{ and} \tag{5}$$

$$X_o = \rho_o c_o A\left(\frac{2\mathrm{H}_1(2k_o a)}{2k_o a}\right). \tag{6}$$

Note once again that no piston structural properties appear in the above equations; they are solely determined by the geometry of the piston and the acoustic properties of the fluid.

We plot the resistance and reactance for a 16.6 mm radius piston in water at the top of Fig. 4. At low frequencies, the resistance (in red) looks like a parabola, while the reactance (in green) looks like a line with a constant slope.

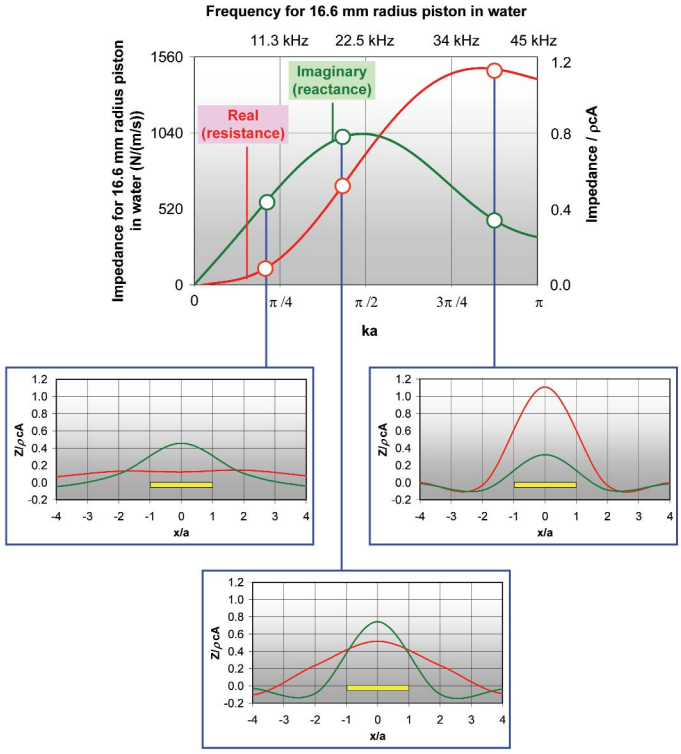


*Fig. 4. Radiation impedance of baffled circular piston. Top–resistance and reactance as a function of frequency (and ka); Bottom–spatial variability of resistance and reactance at three discrete frequencies.*

Popular approximations for the low-frequency resistance and reactance are:

$$R_o \cong \frac{\rho_o c_o A(2k_o a)^2}{8}, \quad (2k_o a)^2 << 1$$
$$X_o \cong \rho_o c_o A\left(\frac{4}{3\pi}\right)(2k_o a). \tag{7}$$

At high frequencies, the resistance asymptotes to a constant value, while the reactance decreases inversely proportionally to frequency:

$$R_o \cong \rho_o c_o A,\ X_o \cong \rho_o c_o A\left(\frac{4/\pi}{2k_o a}\right);\ (2k_o a)^2 >> 1\ . \tag{8}$$

Now, notice how $R_o$ and $X_o$ in the example are plotted in absolute terms, but also plotted normalized against $\rho_o c_o A$ (see the axis on right side of the plot) and against dimensionless frequency *ka* (see the axis on the bottom of the plot). Recall that you can use *ka* to visualize how many acoustic wavelengths fit over the characteristic dimension *a*. In our plot, the maximum *ka* is π, which corresponds to a half wavelength over the piston radius, or a full wavelength across the piston diameter. $R_o / \rho_o c_o A$ converges to a value of 1 at high frequencies. In fact, $R_o / \rho_o c_o A$ is called the normalized radiation resistance, or more commonly, the *radiation efficiency*:

$$\sigma_{rad} = \frac{R_o}{\rho_o c_o A} = \frac{P_{rad}}{\rho_o c_o A\left\langle |v|^2 \right\rangle}. \tag{9}$$

We will learn more about radiation efficiency when we discuss how sound is radiated by plate modes.

At the bottom of Fig. 4, examples of how the fluid loading varies over the surface of a piston are shown at low, mid, and high frequencies. Below a *ka* of π/2, the fluid loading is primarily reactive, or mass-like, weighing down the piston. Above *ka* of π/2, the fluid loading becomes more resistive, absorbing energy in the form of sound from the vibrating structure.

Now, let us suppose that the piston is the mass element of a simple harmonic oscillator, where the mass (*m*) rests on a grounded spring (*k*) and dashpot (*b*). We now consider the effect of the complex fluid loading on the piston resonance, where the piston mobility in-vacuo is:

$$\frac{v}{F} = \frac{1}{i\omega m + b - ik/\omega}\ . \tag{10}$$

The fluid loading (resistance $R_o$ and reactance $X_o$) may be added to the mobility equation to produce:

$$\frac{v}{F} = \frac{1}{i(\omega m + X_o) + (b + R_o) - ik/\omega} \tag{11}$$

For a 1 gram piston of 16.6 mm radius, with spring constant $k$=1x10$^5$ N/m, and a damping constant *b* of 1, we compute the drive point mobility *v*/*F* in air (ignoring fluid load-

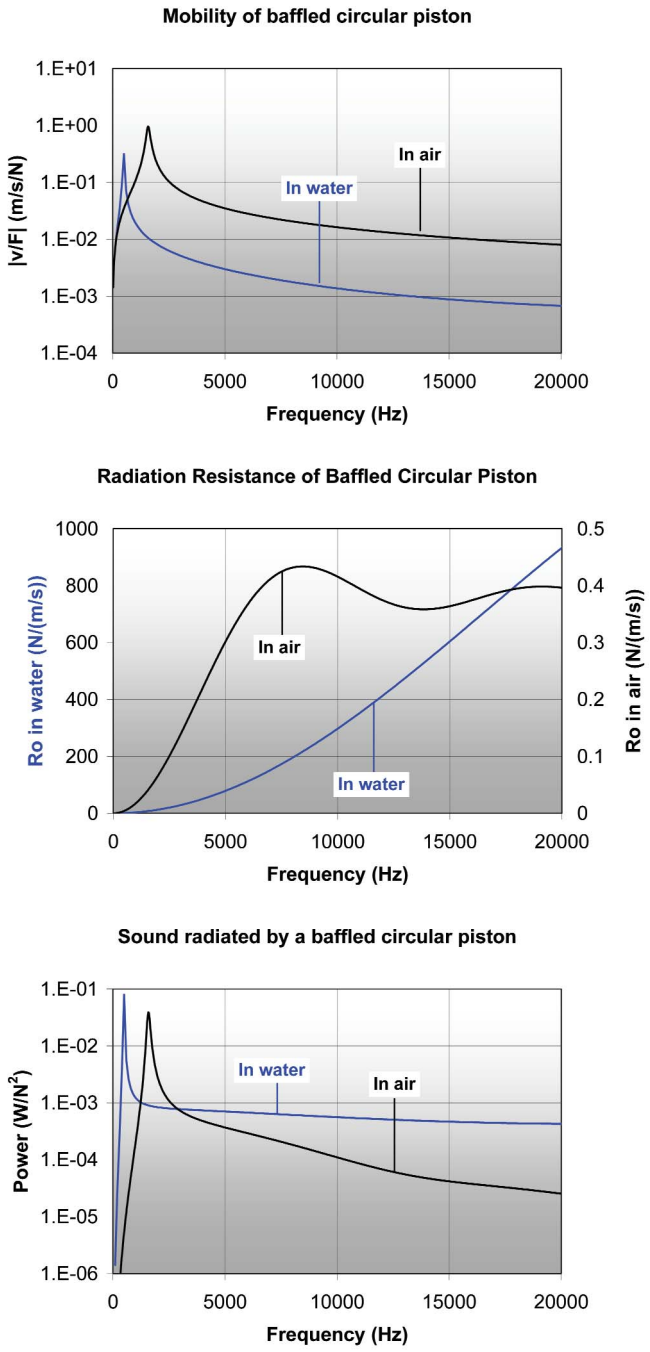


*Fig. 5. Mobility magnitudes (top), radiation resistances (middle), and radiated sound power transfer functions (bottom) of a 16.6 mm radius circular baffled piston in air (black) and in water (blue).*

ing, using Eq. 10), and in water (including fluid loading using Eq. 11). Next, we multiply $R_o$ by the square of mobility to compute radiated sound power. Plots of the mobility magnitude, radiation resistance (in air and in water), and the radiated sound power for a unit force input are shown in Fig. 5.

The effect of mass loading on the piston in water is pronounced, shifting the piston resonance frequency downward, and the overall mobility amplitude downward. The radiation resistance (and reactance) of water is much higher than that of air (be sure to note the multiple scales used on the resistance comparison plot). Therefore, radiated sound power is quite different in air and in water, and the piston resonance peaks occur at different frequencies.

The radiated sound power curve in water illustrates the basic principle of loudspeaker design: adjust the piston properties to set the fundamental resonance as low in frequency as possible, so that the piston response is controlled by the mass term in Eq. 11. Recall that the radiated sound power is the product of the radiation resistance $R_o$ and the square of the piston normal velocity. Since $R_o$ at low $ka$ is proportional to $(ka)^2$, and the piston mobility above resonance is proportional to $1/\omega^2$, the frequency dependencies cancel, leaving a nearly frequency independent radiated sound power/$F^2$ response.

In our example in Fig. 5, the in-air radiated sound power transfer function is not flat above the piston resonance frequency because the radiation resistance is above the frequency range where it is proportional to $(ka)^2$. To resolve this, a speaker designer would simply reduce the radius of the piston, shifting the radiation resistance curve further out in frequency. This solution comes with a cost though—the radiation resistance amplitude reduces with surface area, which will in turn reduce the radiated sound power.

## Structural waves vibrating against an acoustic fluid

How well do structural waves (rather than rigid oscillators) radiate sound? Since only structural motion normal to an object's surface induces an equal motion in a neighboring fluid, we consider transversely vibrating, or flexural waves (we acknowledge, however, that longitudinal waves deform a structure transversely due to an elastic material's Poisson effect, but do not focus on the sound radiated by longitudinal waves here).

How well flexural waves in a structure radiate sound depends on whether the waves, which essentially act as a source against the fluid, are subsonic (slower than the wavespeed in the fluid) or supersonic (faster than the wavespeed in the fluid). Supersonic waves radiate sound, and subsonic waves do not.

Many structural acousticians like to consider the sound radiated by structural waves in wavenumber space, and examine wavetypes on frequency-wavenumber plots. Consider the traveling flexural waves in an infinite plate shown in Fig. 6. The flexural and acoustic wavenumbers (computed by dividing radial frequency by the flexural and acoustic wavespeeds) are plotted against frequency in the top of the figure. Since the acoustic waves are non-dispersive, the wavenumber curve has constant slope. The flexural waves, however, are dispersive, causing a varying slope in the wavenumber curve.

At low frequencies, the structural wavenumbers are higher than those in the acoustic fluid, corresponding to subsonic structural waves. These flexural waves radiate no sound at all (this is only true for infinite plates—we will discuss the sound radiated by finite plates soon). This is because the particle velocity in the fluid normal to the structure's surface must match that of the structure. At low frequencies, acoustic waves are faster than structural ones, so their wavelengths are longer. This means the structure simply cannot induce a propagating wave in the fluid.

The frequency at which the flexural and acoustic waves have the same wavenumber (and wavespeed, and wavelength) is called the *coincidence frequency*, and the flexural

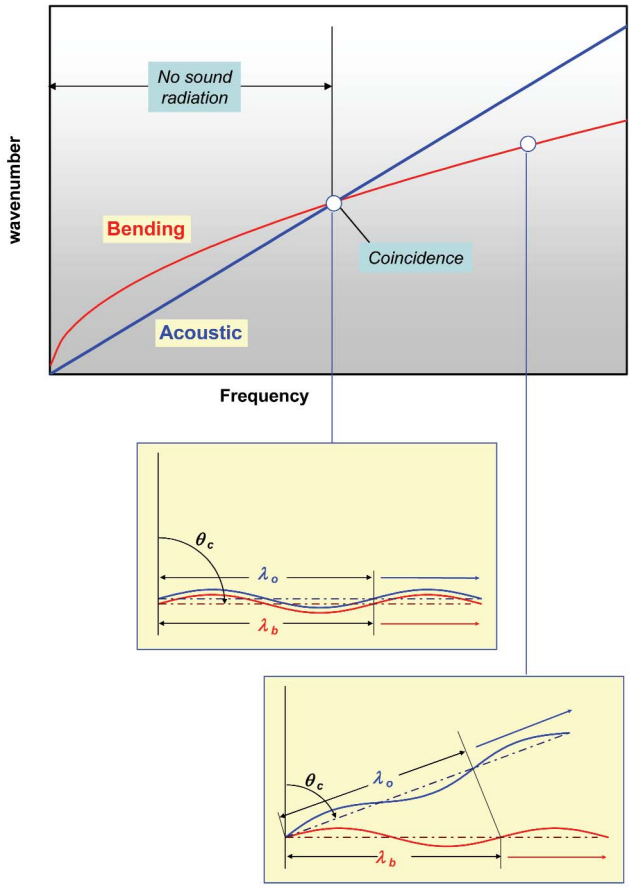


*Fig. 6. Bending and acoustic wavenumber-frequency plot, with trace diagrams of bending and acoustic waves at and above coincidence. Below coincidence, an infinite bending wave radiates no sound!*

waves now radiate sound, as shown in the image in the middle of Fig. 6. They do so in the plane of the plate, or *grazing* the plate. At frequencies above coincidence, the flexural waves continue to speed up—eventually becoming pure shear waves at very high frequencies (see Part 1 of this article). At these high frequencies, the sound radiated by the flexural waves propagates in a preferred direction, which is computed by trace matching the flexural wave to the shorter acoustic wave, as shown in the image on the bottom right of Fig. 6.

The angle of dominant radiation (taken from a vector normal to the structure's surface) is computed as:

$$\theta_c = \sin^{-1}\left(c_o / c_B\right), \tag{12}$$

where $c_B$ is the flexural wavespeed. You can compute a plate's coincidence frequency by setting the flexural and acoustic wavespeeds (or wavenumbers) equal to each other. For bending waves in thin plates at coincidence:

$$c_o = c_B = \sqrt[4]{\frac{D}{\rho h}\omega_c^2}\text{, so} \tag{13}$$

$$\omega_c^2 = c_o^4\frac{\rho h}{D}\text{, or } \omega_c = c_o^2\sqrt{\frac{\rho h}{D}}\ . \tag{14}$$

How does coincidence frequency vary with plate parameters? To find out, let us examine Fig. 7. Increasing a plate's elastic moduli (Young's Modulus $E$ and Shear Modulus $G$) speeds up flexural waves, and lowers the plate's coincidence frequency. Increasing a plate's density increases its mass, slowing down flexural waves, and raises the plate's coincidence frequency. Increasing thickness increases both stiffness and mass, but increases the stiffness at a greater rate, so thickening a plate will lower its coincidence frequency.

Therefore, stiffening a plate lowers its coincidence frequency, allowing it to radiate sound at lower frequencies. Conversely, mass-loading a plate raises its coincidence frequency, so that the plate does not radiate sound at low frequencies. It would seem that the answer to most noise control problems would be to simply add mass to a plate while reducing its stiffness! While this is a good way of reducing sound radiation, we have never had any of our sponsors accept it. As most of us have experienced, nearly all new structures are lightweight and stiff, like carbon-fiber composites reinforced with ribbing. These sorts of structures typically have low coincidence frequencies, and therefore radiate sound very well. Also, as we will see later, lightweight stiff structures are very easy to excite by sound waves.

Since most practical structures are finite, we will now explain how well the mode shapes of a structure radiate (see Part 1 of this article for a discussion of structural resonances). The classic example studied by early structural acousticians is our old friend—the simply supported rectangular plate.

Before we proceed with modal sound radiation, remember a key concept: the standing waves in a mode shape are comprised of multiple left and right (and forward and back) traveling waves, which propagate at the structure's wave speed. It is these traveling waves that radiate, or do not radiate sound. If our plate were infinite, such that there were no reflections from any of the plate boundaries, subsonic flexural waves would radiate no sound. However, the discontinuities at the boundaries 'scatter' the energy in subsonic flexural waves into many wavenumbers, some of them supersonic, so that a finite plate radiates sound below its coincidence frequency. The amount of sound radiation depends on the radiation efficiency of each of the plate's modes.

Maidanik[7] and Wallace[8] computed how much sound a finite rectangular simply supported plate's modes radiate. In particular, Wallace provides formulas for the frequency-dependent far-field pressure and acoustic intensity fields radi-

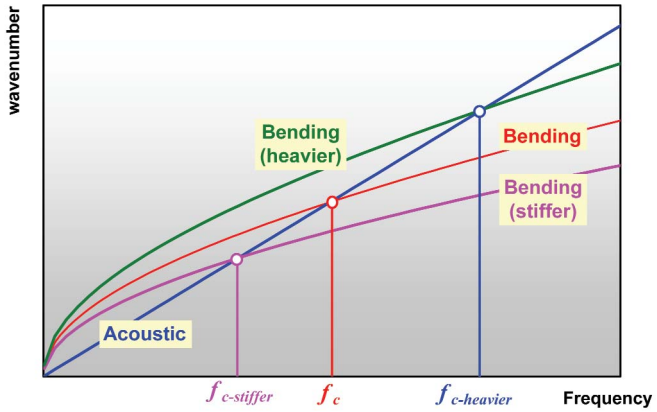


*Fig. 7. Effects of stiffening and mass-loading on plate coincidence frequencies. Stiffening a plate reduces the coincidence frequency, and adding mass increases it.*

ated by a given plate mode, along with an integral for computing the sound power radiation efficiency for each mode. We show the far-field intensity below, near, and above the plate coincidence frequency for the first three low-order modes of a square 1m x 1m plate in Fig. 8. Recall from the first article that we define mode orders as (*m*, *n*) pairs, where *m* and *n* correspond to the number of antinodes (regions of maximum deformation) in the plate's *x* and *y* directions, respectively.

In the figure, the mode shapes of the plate are shown, along with the corresponding far-field intensity patterns. At low frequencies, the fundamental (1,1) mode radiates sound omnidirectionally, like a baffled circular piston. Also at low frequencies, the (1,2) mode radiates sound like a dipole, and the (2,2) mode radiates like a quadrupole.

The figure also shows radiation efficiencies as a function of acoustic wavenumber (frequency/acoustic wavespeed), with a line shown to indicate the frequencies of the directivity plots. Notice how they resemble the normalized radiation resistance of the baffled circular piston (Fig. 4). Below coincidence, the efficiencies increase rapidly with increasing frequency. The efficiencies peak at coincidence (exceeding 1, showing that they are not true efficiencies!), and then asymptote to a value of one above coincidence.

Above coincidence, the far-field sound directivity changes, with 'lobes' of sound radiated from the structure at critical angles. These critical angles may be computed using the trace matching procedure described above for the infinite plate. The critical angles exist for all plate modes except the fundamental (1,1) mode, which radiates sound normal to the plate at all frequencies, but with a spatial 'beamwidth' that narrows with increasing frequency.

Let us re-examine the radiation efficiencies below coincidence for the different mode orders. We see that the (1,1) mode radiates sound most efficiently, followed by the (1,2) mode, and then the (2,2) mode, which radiates sound least efficiently. This trend shows an important result: modes with odd *m* and *n* orders radiate sound much better than those with mixed orders (odd-even or even-odd), which radiate better than those with purely even orders (even-even).

Using the analytical radiation efficiencies, we can compute how much sound a rectangular plate radiates when driven by a point force. To do so, we combine the mobility formula from Part 1 of this article with radiation efficiencies computed using the formulas in Wallace.[8] Ignoring any fluid loading effects on the structure (which we know will mass-load and radiation damp the structure from our exercises with the baffled circular piston), we show the mobility, radiation efficiency, and radiated sound power for a unit force drive in Fig. 9.

Starting with the mobility (top of the figure), we see how the contributions from the individual modes compare to the total mobility. The mobility is dominated by resonant response at the resonance frequencies, and a mix of non-resonant responses away from resonance.

Next, examining the radiation efficiencies of the modes shows the same trends we observed in Fig. 8—that odd-odd modes radiate sound very well, but modes with mixed and even orders radiate sound poorly. The fundamental (1,1) mode radiates sound very much like a baffled piston, and the

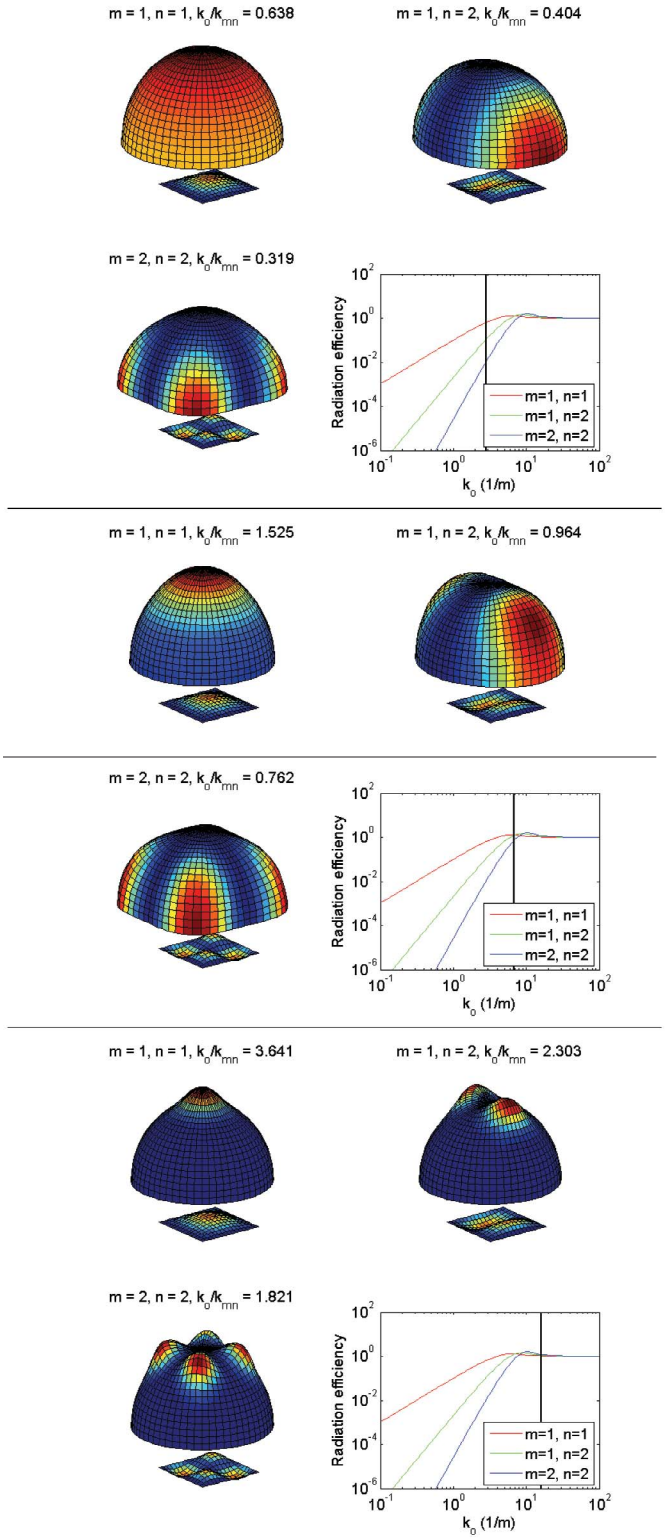


*Fig. 8. Far-field sound intensity in air for various low-order simply supported 1 m square flat plate modes. Top–below coincidence, Middle–near coincidence, Bottom–above coincidence.*

radiated sound power transfer function (power normalized by the square of the input force) is dominated by the sound radiated by that mode. Peaks in the sound power occur for the other modes, primarily the other odd-odd (1,3) mode, but the non-resonant sound radiated by the (1,1) mode is nearly flat with increasing frequency.

This example brings up one of the key points of this arti-

cle—*non-resonant sound radiation can be higher than resonant sound radiation*. The sound radiated by the (2,2) mode at its resonance frequency just below 100 Hz is a good example—it is lower than the non-resonant sound radiated by the (1,1) mode!

When we coupled the radiation resistance of a baffled piston to a simple harmonic oscillator (where the piston head was the mass), we added it to the resistance of the oscillator. For finite structures, most analysts use mechanical loss factors to model structural damping. We can compute a *radiation loss factor* which can be used in a structural analysis to represent the radiation damping of an acoustic fluid. A useful equation for the radiation loss factor of a uniform thickness, homogenous plate or shell structure (flat or curved) is

$$\eta_{rad} = \frac{\rho_0}{\rho_s} \frac{1}{k_0 h} \sigma \ . \qquad (15a)$$

The equation shows that the radiation loss damping is directly proportional to fluid density, meaning that the heavier the fluid, the more sound power is radiated, and the more heavily damped the structure. An example would be a vibrating bell dunked in water. While in the air, the bell's vibrations would 'ring' for a long time. When immersed in water, the vibrations decay quickly. An extension of the above equation, well known in the Statistical Energy Analysis (SEA) community, relates the radiation loss factor to the radiation resistance:

$$\eta_{rad} = \frac{\rho_0}{\rho_s} \frac{1}{k_0 h} \left( \frac{R_o}{\rho_o c_o A} \right) = \frac{R_o}{\omega \rho_s h A} = \frac{R_o}{\omega M} \ , \qquad (15b)$$

where $M$ is the mass of the plate or shell.

Table 1 provides a useful list of the various sound radiation quantities and how they inter-relate.

## The complementary problem—Structural vibrations induced by acoustic pressure waves

Whereas the sound radiated by vibrating objects is often just an annoyance, the vibrations induced in structures by impinging acoustic waves can be so high that the structures crack and fail. This is clearly a more serious problem, and has

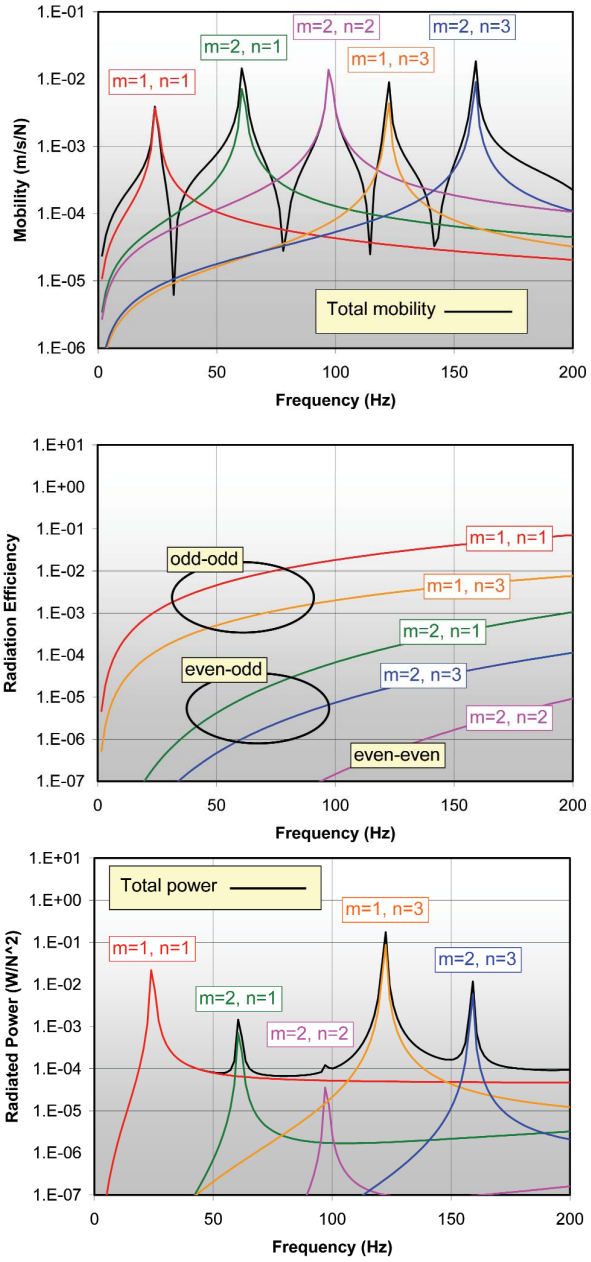


*Fig. 9. Mobility magnitude (top), radiation efficiency (middle), and radiated sound power transfer function (bottom) of a simply supported 1m square 5 mm thick flat steel plate in water driven at its quarter point (x=0.25 m, y=0.25 m).*

*Table 1. List of sound power radiation quantities and their interrelationships.*

| | Sound Power ($P_{rad}$) | Radiation Resistance ($R_o$) | Radiation Efficiency ($\sigma_{rad}$) | Radiation loss factor ($\eta_{rad}$) |
|---|---|---|---|---|
| Sound Power | - | $P_{rad} = R_o \left\langle \lvert v \rvert^2 \right\rangle$ | $P_{rad} = \sigma_{rad} \rho_o c_o A \left\langle \lvert v \rvert^2 \right\rangle$ | $P_{rad} = \eta_{rad} \omega M \left\langle \lvert v \rvert^2 \right\rangle$ |
| Radiation Resistance | $R_o = \frac{P_{rad}}{\left\langle \lvert v \rvert^2 \right\rangle}$ | - | $R_o = \sigma_{rad} \rho_o c_o A$ | $R_o = \eta_{rad} \omega M$ |
| Radiation Efficiency | $\sigma_{rad} = \frac{P_{rad}}{\rho_o c_o A \left\langle \lvert v \rvert^2 \right\rangle}$ | $\sigma_{rad} = \frac{R_o}{\rho_o c_o A}$ | - | $\sigma_{rad} = \eta_{rad} \frac{\rho_s}{\rho_o} k_0 h$ |
| Radiation Loss Factor | $\eta_{rad} = \frac{P_{rad}}{\omega M \left\langle \lvert v \rvert^2 \right\rangle}$ | $\eta_{rad} = \frac{R_o}{\omega M}$ | $\eta_{rad} = \sigma_{rad} \frac{\rho_0}{\rho_s} \frac{1}{k_0 h}$ | - |

been studied intently by those in the aerospace and nuclear communities, particularly in the 1960's and 1970's.

Try holding your hand or fingers lightly on any structural surface, like a window when there is a lot of noise outside. You will feel the window vibrating. The physics that explain this phenomenon are the same as those that explain how a vibrating structure radiates sound. As we will see, there are several quantities in sound-induced vibration that are complementary to those in vibration-induced sound.

Let us start by considering the acoustic field adjacent to a flat infinite plate that is struck by an incoming acoustic wave. There are many pressure waves next to the structural surface—the incident wave, a reflected wave, and a wave re-radiated by the structure, which has been forced into vibration by the incident and reflected waves. The sum of the incident and reflected waves forms a 'blocked' pressure on the surface, and if the surface is rigid, the blocked pressure field is the total pressure. If the structure is flexible and vibrates, it radiates a third pressure wave, which sums with the blocked pair to form the overall pressure field.

Figure 10 shows the incident and reflected waves for a 30 degree angle of incidence (the angle is taken from the direction normal to the plate), along with the total blocked pressure field acting on a rigid surface. Notice how the two waves combine to form a standing wave pattern in the direction normal to the surface. The standing wave pattern propagates in the direction parallel to the surface at a speed $c_o \sin(\phi)$, where $\phi$ is the angle of incidence.

Infinite plate theory (discussed in Part 1 of this article) can be used to estimate the plate vibration caused by the blocked pressure field:

$$v_n = \frac{2\,p_{incident}}{z_{fluid} + z_{plate}} \,, \tag{16}$$

where $z_{\phi\lambda\upsilon\iota\delta}$ and $z_{\pi\lambda\alpha\tau\varepsilon}$ are the impedance (pressure/velocity in this case) of the acoustic space and the plate.

The fluid impedance depends on the pressure wave's angle of incidence and the fluid's characteristic impedance:

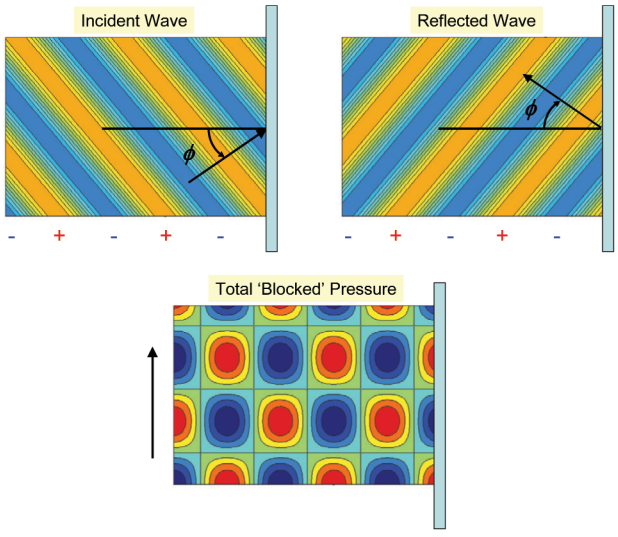


*Fig. 10. Blocked pressure field acting on a plate (right side of images) at 30 degree angle of incidence. '+' and '–' signs indicate phase variations in the waves.*

$$z_{fluid} = \rho_o c_o / \sqrt{1 - \sin^2 \phi_{incident}} \,, \tag{17}$$

and the infinite plate's impedance is

$$z_{plate} = D(k_o \sin\phi_{incident})^4 \eta / \omega - i\left[ D(k_o \sin\phi_{incident})^4 - \rho h \omega^2 \right] / \omega \,, \tag{18}$$

where $\eta$ is the structural loss factor and $h$ is the plate thickness.

Examining the equation, we can see that the plate will vibrate most when its structural impedance is minimized. This will occur when the stiffness and mass terms in the plate's impedance cancel each other, or when $D(k_o \sin\phi_{\iota\nu\chi\iota\delta\varepsilon\nu\tau})^4 = \rho h \omega^2$ Let us find this frequency. To do so, we replace $k_o$ with $\omega/c_o$, and we find that:

$$\omega_{co} = \sqrt{\frac{\rho h}{D}} \frac{c_o^2}{\sin^2 \phi_{incident}} \,. \tag{19}$$

$\omega_{\chi o}$ looks similar to a plate's critical frequency, and to its critical radiation angle for frequencies above coincidence. In fact, when $\phi_{\iota\nu\chi\iota\delta\varepsilon\nu\tau}$ is 90 degrees (the acoustic waves propagate in the plane of the plate, or 'graze' the plate), the coincidence frequency is the critical frequency. The critical frequency, in fact, is sometimes called the lowest coincidence frequency. This means that there is no single frequency where the plate vibrates most—there are several of them, each of which correspond to a different angle of incidence.

Now let us consider how finite structures respond to incident acoustic waves. However, we will do so not for waves that are incident from specific angles, but for groups of waves that are statistically incident from all angles, more commonly known as a *diffuse acoustic field*. Smith[9] considered how a simple harmonic oscillator responds to diffuse acoustic fields in 1962, where the mean square velocity response of the oscillator is

$$\frac{M\left\langle v^2 \right\rangle}{G_{pp}} = \frac{2\pi^2 c_o}{\rho_o \omega^2} \left( \frac{R_{radiation}}{R_{structure} + R_{radiation}} \right) \,, \tag{20}$$

where $M$ is the oscillator mass, $R_{\rho\alpha\delta\iota\alpha\tau\iota o\nu}$ and $R_{\sigma\tau\rho\upsilon\chi\tau\upsilon\rho\varepsilon}$ are the radiation and structural resistances, and $G_{\pi\pi}$ is the autospectrum of the incident pressure.

The randomly excited simple harmonic oscillator problem is one of the origins of Statistical Energy Analysis (SEA), a popular structural-acoustic analysis technique. For multi-resonant structures, like plates, the plate energy is computed rather than velocity:

$$\frac{\left\langle E \right\rangle_{plate}}{G_{pp}} = \frac{2\pi^2 c_o n_{plate}}{\rho_o \omega_{center}^2} \left\langle \frac{R_{radiation}}{R_{structure} + R_{radiation}} \right\rangle_{\omega_{\min} \to \omega_{\max}} \tag{21}$$

Here, the radiation and structural resistances are averaged over a frequency band spanned by $\omega_{\mu\iota\nu}$ and $\omega_{\mu\alpha\xi}$. Also, we include the modal density $n_{\pi\lambda\alpha\tau\varepsilon}$, which defines the number of plate modes in the frequency band. As we can see, SEA is statistical, averaging over bands of frequencies. SEA also

computes averages of response over space, since $\langle E \rangle_{\text{πλατε}}$ is averaged over the plate.

A full discussion of SEA is outside the scope of this tutorial, but you can find more information on SEA in the review paper by Burroughs[10] and a more thorough treatment of how structures respond to diffuse fields in the article by Shorter and Langley.[11]

You can use Eq. 21 without using SEA, though. You just need to know the incident pressure spectrum of the diffuse acoustic field, and the radiation and structural resistance. You also need an estimate of the plate's modal density, which is

$$n_{plate}(\omega) = \frac{A_{plate}\omega}{4\pi c_B^2}, \tag{22}$$

Note that the plate's modal density depends on frequency (as do all modal densities).

Examining the equation, we see that the higher the radiation resistance, the higher the plate energy (and therefore the higher the plate's vibration). So, the better a plate radiates, the easier it is to excite with incident pressure fields!

Now, what happens when there is also fluid on the other side of the plate? How much of the incident sound gets through the plate to the other side? This is the classic sound transmission loss problem, and may be solved easily for an infinite plate, and not so easily for a finite one.

Fahy[4] provides a derivation of the sound power transmission coefficient through an infinite plate in his textbook, and we repeat it here (assuming the fluids on both sides of the plate are the same):

$$\tau = \frac{\left[2\rho_0 c_0/\sin\phi\right]^2}{\left[2\rho_0 c_0/\sin\phi + (D/\omega)\eta\left(k_0\sin\phi\right)^4\right]^2 + \left[\omega\rho h - (D/\omega)\left(k_0\sin\phi\right)^4\right]^2}. \tag{23}$$

The red, green, and blue terms in the equation represent the damping, mass, and stiffness of the plate, respectively. The amount of sound transmitted depends on the fluid properties, the structural properties, frequency, and the angle of the incident pressure wave with respect to the plate.

Some typical transmission loss plots, computed as $10\log_{10}(1/\tau)$ are shown in Fig. 11. For acoustic waves not normally incident to the plate, sharp dips appear in the transmission loss. These dips correspond to sharp peaks in the transmission coefficient (transmission loss is the inverse of the transmission coefficient), and act as strong pass-bands of incident sound. The dips are at the coincidence frequencies of the plate. Recall that the coincidence frequencies depend not only on the plate, but on the angle of incidence of the sound waves. As the angle of incidence changes, the coincidence frequency and the frequency of the transmission loss dip changes as well.

At low frequencies, the mass term in Eq. 23 determines the transmission loss, which increases with the square of frequency (6 dB/octave, or 6 dB for each doubling of frequency). At high frequencies, above the coincidence dip, plate

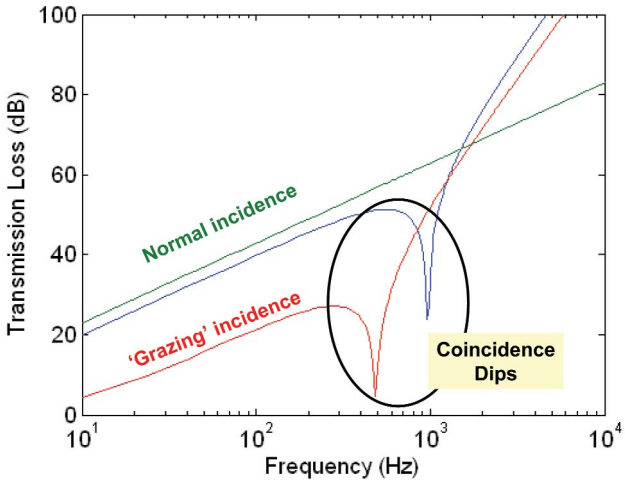


*Fig. 11. Typical transmission loss plot for variable angles of incidence. Grazing incidence refers to acoustic waves that are nearly in the plane of the plate.*

stiffness is dominant, and the transmission loss increases with the 6th power of frequency, or 18 dB/octave. Figure 11 shows what most people already know from experience—it is hard to keep low-frequency sounds from propagating through barriers. Consider this the next time you close a door to block out sound from a hallway or another room. You stop hearing mid-high frequency sounds, but still hear 'muffled' low-frequency noise.

To visualize the sound field incident on and transmitted by an infinite plate, Fig. 12 compares pressure and displacement of a plate at two conditions: well below, and near coincidence. In the example, we have set the plate loss factor equal to 0. Try setting loss factor to zero and computing the transmission coefficient in Eq. 23 at coincidence (remember, this is where the acoustic wavenumber in the plane of the plate matches the free bending wavenumber in the plate, or $k_o \sin\phi = k_\beta$). You should compute a transmission coefficient of 1, which is perfect sound transmission!

The strength, or depth of the coincidence dip depends strongly on the plate's loss factor η. Designers of noise barriers (windows, doors) try hard to minimize the depth and breadth of the coincidence dips. The most common approach for mitigating coincidence dips is using constrained layer damping, or CLD (we learned about this in Part 1 of this article). Automotive glass in luxury vehicles, and glass in high-end office buildings usually have a thin layer of clear vinyl sandwiched between two panes of glass.

For zero, or normal angle of incidence (sound waves normal to the plate's surface), the transmission coefficient is not indeterminant (you might think it would be, since there are several terms in Eq. 23 that divide by sin(ϕ)). The transmission coefficient actually simplifies to:

$$\tau_{\phi=0} = \frac{1}{1 + \left(\frac{\omega\rho h}{2\rho_o c_o}\right)^2}, \tag{24}$$

which corresponds to the well-known 'mass law.' The mass law transmission loss is shown in green in Fig. 11, and increases with the square of frequency over all frequencies,

never showing a coincidence dip.

To improve transmission loss, many noise control engineers use two panels, particularly in windows. Called 'double glazing,' the panels are separated by an air (or other gas) gap. Since transmission loss is additive, there is a substantial improvement, much more so than simply increasing the thickness of a single panel. However, most double panel systems have different panel thicknesses so that the coincident dips of the two panels occur at different frequencies. While this leads to two pass-bands for incident sound, it is generally preferable to have two weak pass bands rather than one very strong one.

In most practical situations, acoustic waves impinging on a panel do not arrive from the same angle. Consider a window in an office building or a hotel. Sound waves arrive from all angles, with a random distribution of the angles over time (imagine incident sound from passing airplanes and automobiles, reflecting off of adjacent buildings). Therefore, statistical methods have been used to estimate a *random angle of incidence* transmission loss for low frequencies:

$$TL_{random} = TL_0 - 10\log_{10}(0.23TL_0) \qquad (25)$$

where $TL_0$ is $10\log_{10}(1/\tau_{f=0})$, or the mass-law normal incidence transmission loss. Since transmission loss is maximized (transmission coefficient is minimized) at normal incidence, the random angle of incidence transmission loss is a fraction of that at normal incidence.

Be careful using the above expression at high frequen-

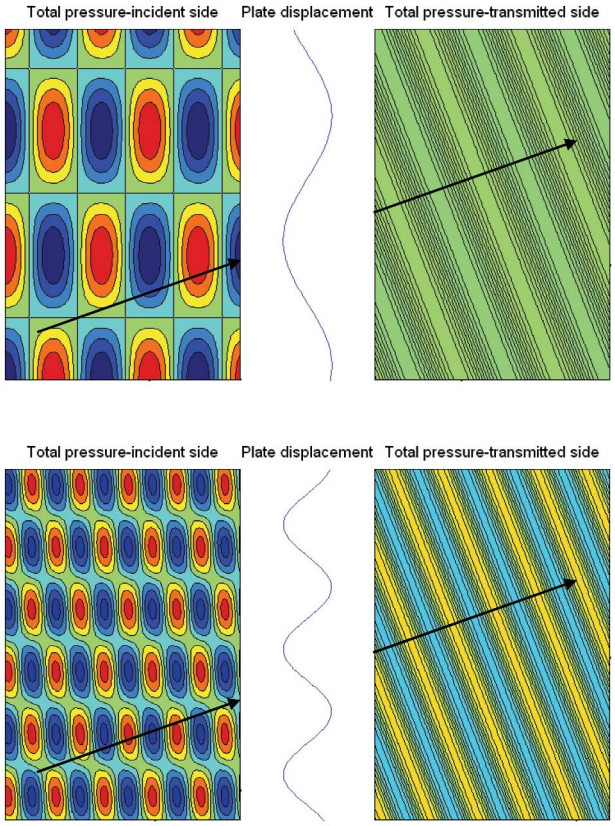


*Fig. 12. Incident and transmitted sound fields around an infinite 25 mm thick steel plate, 30 degree angle of incidence. Top–at 50% of coincidence, Bottom–at coincidence. Dark blue and red indicate high pressures, and green indicates low pressures.*

cies! It does not include the coincidence dip, or the high-frequency stiffness effects. To consider these effects, and those of finite panel boundaries, other techniques are used, like SEA. In fact, one of the early SEA applications was for single and double panel transmission loss calculations. Price and Crocker's famous papers[12, 13] clearly show the coincidence dips in transmission loss, and the importance of varying panel thicknesses in double panel systems.

## Measurements of sound—structure interaction

The sound radiated by vibrating structures, and conversely, the vibrations induced in structures by sound fields, are commonly measured in two types of chambers: reverberation rooms, and anechoic rooms. Interconnected rooms are used to measure the transmission loss of barriers, like windows and doors.

Accelerometers mounted to structures can provide a spatially averaged normal velocity. Also, non-contact velocity measurements are often made using laser vibrometry, eliminating the mass-loading effects of the accelerometers on the test structure, and reducing test times.

Measuring sound power is more difficult than measuring vibration. In air, arrays of microphones may be used to measure the spatial variability of pressure. In water, hydrophones are used. Sound pressures are measured quite differently in reverberant and anechoic rooms, though.

In a reverberant room, the acoustic modes of the air in the room are excited by a vibrating structure. When the acoustic cavity modal density is high, the room's pressure field becomes nearly diffuse, such that pressures measured at just a few locations randomly spaced throughout the room may be used to estimate the total sound power radiated by a vibrating object. The sound power is computed using the measured pressures, along with a few of the reverberation room's parameters, such as the volume and the *reverberation time*. The reverberation time is inversely proportional to the room's loss factor—the longer a pressure impulse takes to decay, the lower the room's loss factor.

The accuracy of a reverberation chamber sound power measurement depends on the room's modal density and reverberation time (among other things). The sound power is actually a statistical mean, which is bracketed by a standard deviation at each measurement frequency. In general, the higher a room's modal density and the wider the frequency bandwidth, the smaller the standard deviation. Most reverberation room sound power measurements are therefore made over wide frequency bands that contain several acoustic modes. One-third octave frequency bands are commonly used.

There are standards[14, 15] available to help an experimentalist quantify a reverberation chamber's characteristics, and conduct a sound power measurement. The standards, however, are specific to rooms filled with air. To make measurements in a reverberant water tank, some modifications to the approaches in the standards are necessary. Conlon describes these modifications, and applies them to ARL/Penn State's reverberant water tank in his NoiseCon 2004 article.[16] Photographs of a metal pressure vessel being tested in ARL/Penn State's tank are shown in Fig. 13. The vessel is struck by an impact hammer at several points, and the pressures measured at five hydrophone locations are used to estimate the sound power transfer function ($P_{\rho\alpha\delta}/F^2$).

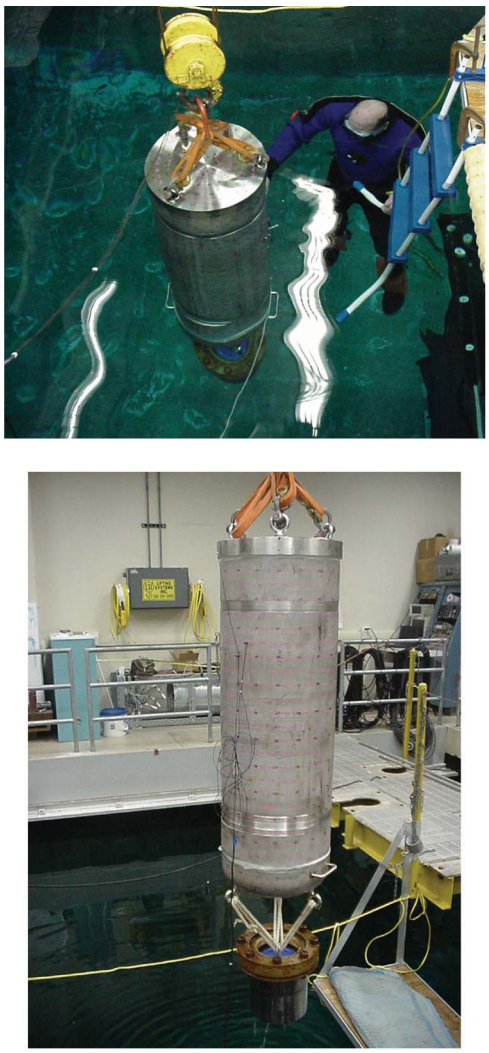

*Fig. 13. Impact hammer measurements on cylindrical shell structure submerged in ARL/Penn State Reverberant Water Tank. Top–shell submerged in tank with diver; bottom, shell suspended over tank.*

The sound power transfer functions for several drive locations on an elbowed pipe (the same pipe described in Part 1 of this article) are shown in Fig. 14, adapted from another NoiseCon article,[17] this one from 2005. The measurements were made in one-third octave bands, and show that the sound power transfer functions vary with drive location (just as mobility functions do). Annotations on the graph show where various shell modes cut on (again, see Part 1 of this article to refresh your memory on what shell modes are).

It is often useful to compare sound power transfer functions to that of an ideal dipole source:

$$\frac{P_{rad\_dipole}}{|F|^2} = \frac{1}{12\pi\rho_0 c_0} k_o^2 \quad , \tag{26}$$

where $|F|^2$ represents the square of the r.m.s. force amplitude. This would be the sound made by an oscillating point drive in space. At some frequencies, most notably those of structural resonance, the sound power transfer function for the elbowed pipe is higher than that of a point dipole, showing that the structure amplifies the force drive at those frequen-

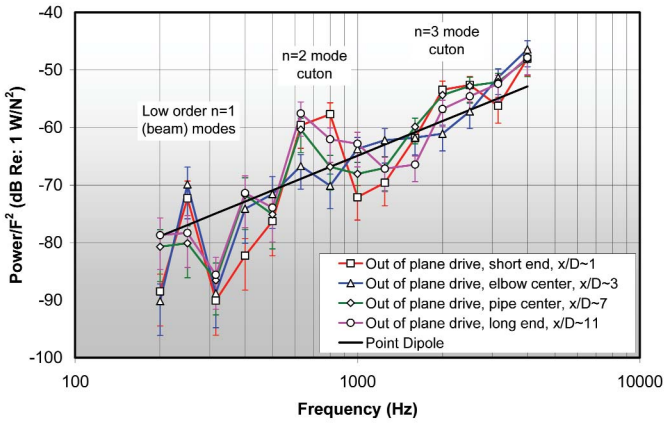


*Fig. 14. Sound power radiated by Schedule 10 Steel 3 inch pipe with elbow, pipe length/diameter~12.*

cies. At other frequencies, usually between structural resonances, the structure attenuates the drive.

The sound power transfer functions can also be combined with a surface-averaged mobility measurement to compute radiation efficiency:

$$\sigma_{rad} = \left(\frac{P_{rad}}{|F|^2}\right)\left(\left\langle\left|\frac{F}{v}\right|^2\right\rangle\right)\left(\frac{1}{\rho_o c_o A}\right). \quad (27)$$

Pressure, intensity, and sound power are measured very differently in anechoic rooms. The walls of a typical anechoic chamber are coated with sound absorption materials. Foam wedges are common, as shown in Fig. 15. The absorbing material nearly eliminates the reflection of sound by the walls. The pressure measured around a sound source placed in an anechoic room is due only to acoustic waves propagating away from the source.

Anechoic environments allow for more refined measurements of sound fields, both over space and frequency. Directivity plots like those in Fig. 3 and Fig. 8 may be measured. Also, narrow-band frequency spectra may be computed. However, whereas only a few pressure measurements are required in reverberant rooms to compute radiated sound power, many more pressure measurements are required to do so in an anechoic room.

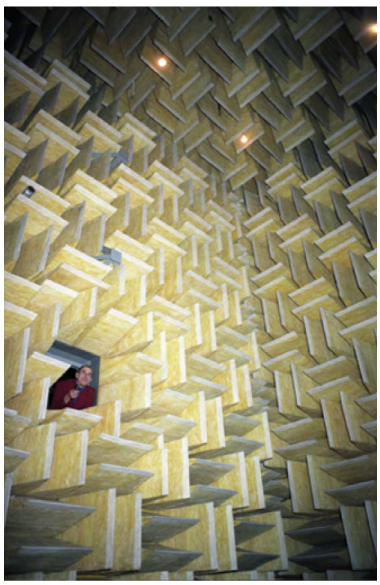

*Fig. 15. ARL/Penn State's Anechoic Chamber.*

Total sound power must be integrated over a closed surface around the sound source. Also, acoustic intensity must be measured, sometimes in the near-field of the structure. This means many intensity measurements are made over several points around the structure. The points may be defined over a hemisphere or a box-like shape. Standards are available[18] to guide your measurements, and acoustic intensity probes, like the one shown in Fig. 16, are widely available.

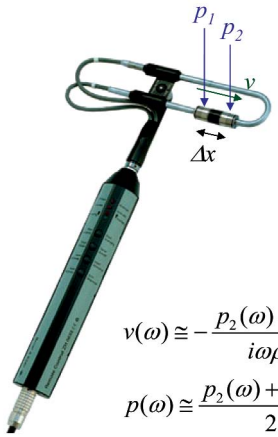


$$v(\omega) \cong -\frac{p_2(\omega) - p_1(\omega)}{i\omega\rho_o \Delta x}$$

$$p(\omega) \cong \frac{p_2(\omega) + p_1(\omega)}{2}$$

$$I(\omega) \cong \mathrm{Re}\left[\frac{1}{2} p(\omega) v^*(\omega)\right]$$

*Fig. 16. Hand-held acoustic intensity probe. Two microphones are separated by a known distance Δx so that particle velocity may be computed using a finite difference approximation. The mean pressure and estimated particle velocity are combined to compute the active, or real part of acoustic intensity in the direction along the x-axis.*

Two measurement chambers are required to determine a barrier's transmission loss. Often, a thick, nearly rigid wall is built between the two rooms. The wall includes an opening, into which a barrier is mounted. One of the rooms is considered the 'source' room, and is ensonified with sound waves, which strike the barrier. The sound power in the 'receiver' room is measured, and a transmission coefficient is calculated. Usually, the source room is reverberant, and the receiver room is anechoic, with measurements made according to the procedures we described above.

## Boundary element modeling of sound fields

Boundary element methods have been used to predict acoustic fields for about 45 years, and there is a vast amount of literature on the subject. Although these methods can be used to compute both interior and exterior acoustic fields, the focus here is on computing exterior acoustic fields where boundary elements have distinct advantages. Since this article is at the level of a tutorial, our main goal will be to give the reader a brief synopsis of the basic analysis techniques and the current state of the art. For the sake of simplicity, the specified boundary condition and radiated acoustic field are assumed to be time-harmonic.

A completely general solution for the pressure field of a

vibrating structure can be derived in the form of an integral equation, which is an equation with an unknown function under an integral sign. Even though we cannot actually solve the integral equation for the unknown function explicitly for any but the simplest problems, it is still useful to know the form of the solution in terms of physical variables. Also, the solution provides great insight into how the problem might be solved numerically, and, as such, the Kirchhoff-Helmholtz integral equation (KHIE) commonly provides the starting point for many numerical formulations:

$$4\pi\, p(\boldsymbol{r}) = -\iint_S \left\{ \begin{matrix} G(\boldsymbol{r},\boldsymbol{q})\left[i\omega\rho v_n(\boldsymbol{q})\right] - \\ p(\boldsymbol{q})\, dG(\boldsymbol{r},\boldsymbol{q})/\, dn_q \end{matrix} \right\} dS(\boldsymbol{q}) \qquad (28)$$

In the KHIE, $\boldsymbol{r}$ represents a point in the acoustic fluid and $\boldsymbol{q}$ is a point on the boundary of the fluid $S$, or boundary surface. In the context of sound radiation from structural vibrations, the boundary surface is the outer surface of the structure in contact with the acoustic medium. The function $G$ stands for Green's function, and $G$ and $dG/dn$ in the KHIE represent the acoustic fields of simple (monopole) and dipole sources, respectively, distributed along the boundary surface. The dipole sources are aligned in the direction perpendicular to the boundary surface. The monopole and dipole sources are functions of the point $\boldsymbol{q}$ where they are located and the field point $\boldsymbol{r}$. The KHIE shows that the acoustic field depends only on what happens at the boundaries since the surface vibrations cause the radiated acoustic field.

By studying the solution for the acoustic field given by the KHIE, much can be learned about how to derive a numerical solution. Unfortunately, its simplicity is deceiving. The acoustic fields of simple and dipole sources are singular functions of the source and field point locations, such that they become infinite when the two points coincide (when $\mathbf{r} \rightarrow \mathbf{q}$ ). However, in the KHIE, these singular functions add together to yield nonsingular pressure and velocity fields. Taking $R$ to be the distance between $\boldsymbol{r}$ and $\boldsymbol{q}$, the singularities for the different sources can be categorized as:

(1) pressure of a simple source $G \sim 1/R$,
(2) velocity of a simple source $dG/dn_0 \sim 1/R^2$,
(3) pressure of a dipole source $dG/dn \sim 1/R^2$,
(4) velocity of a dipole source $d(dG/dn_0)/dn \sim 1/R^3$.

The process of taking a derivative makes a singular function more singular. For example, taking the derivative of $r^{-1}$ with respect to $r$ gives $-r^{-2}$. When $r$ is less than unity, the function $r^{-1}$ is smaller than $r^{-2}$, so that $r^{-2}$ goes to infinity faster as $r \rightarrow 0$. A function that depends on $1/R$ is called weakly singular, one that depends on $1/R^2$ is called strongly singular, and one that depends on $1/R^3$ is called hyper-singular.

How is it possible, then, for singular functions to add up to give finite pressure and velocity fields? First, integration is a "smoothing" operation. Thus, it tends to reduce the level of singularity, the same way differentiation increases it. Because the functions are integrated over a surface, this process essentially reduces the level of singularity by two orders. Thus, it makes sense that weakly and strongly singular functions should yield finite values. However, we would not expect a hyper-singular function integrated over a surface to yield a finite value. Indeed, the only reason the velocity field of a dipole source yields a finite value is because the surface pressure and normal velocity, which are weighting functions for simple and dipole sources, are related through a gradient operation. To illustrate, consider a right-angled corner, where the surface normal is discontinuous. As we travel along the surface towards the corner, the pressure field must change such that the gradient operation produces the correct velocity on the other side of the corner.[19] The level of continuity in the pressure field is also important. In the exact solution, the surface pressure is an absolutely continuous function, such that the function itself, as well as all of its derivatives, are continuous. This level of continuity is impossible to duplicate with simple polynomial approximations. However, the pressure and surface velocity, taken together, must enforce $-i\omega\rho\, \boldsymbol{v} = -\nabla p$ as we travel along the boundary. Thus, it is impossible to duplicate the level of continuity in the actual surface pressure distribution with simple interpolation functions and it is also impossible to exactly enforce the specified boundary conditions!

From a practical point of view, how is all this relevant? First, many of the research papers written about boundary element methods in the last ten years are concerned with sorting out the mathematical details of the integrals. These papers are written by, and for, people writing their own boundary element codes. A novice would find it very difficult to understand all the mathematical complexities. (Admittedly, even after years of dedicated effort, we find many of the papers incomprehensible.) A reader interested in a simple explanation of boundary element methods will find the earliest papers on the subject, written in the 60's, much easier to understand.[20, 21, 22] Also, for the casual users who are not trying to write their own boundary element code, it is only important to understand that current boundary element codes are not perfect. They probably do not take care of the singularities in the KHIE such that the acoustic field is strictly non-singular. Nonetheless, it has been well shown over the years that even simple approximations for the pressure and normal surface velocity weighting functions yield adequate numerical solutions for many problems.[22]

After constructing and solving the matrix system, the pressures and normal velocities are known for each element of the boundary surface. The KHIE can then be used to directly compute the pressure at each desired field point location. The overall sound power output can be computed by setting up a grid of field point locations on a surface enclosing the structure and numerically integrating the acoustic intensity over the surface. In theory, the power output can also be computed directly using the pressure and normal velocity on the boundary surface, but this is problematic because this is where the largest errors tend to occur in a boundary element solution.

Aside from the mathematical details in evaluating the integrals, most recent innovations in boundary element methods have concerned ways to increase the speed of the computations and reduce storage requirements. As with all numerical computations, boundary element methods have

benefited enormously from the rapid increase in computer processor speed and memory. Since boundary element computations are repeated many times at different frequencies, it is easy to split jobs up and assign them to different computers or processors.

In practice, boundary element methods are very competitive for all but the very largest engineering problems, where the matrix inversion and multiplication dominate the solution times. This is especially true if the time required to create models is factored into the analysis. In this respect, boundary element methods are relatively quick and easy. Simple rules of thumb can be used to determine if boundary element methods will be applicable for a specific problem. Generally, six elements are required per acoustic wavelength to accurately compute an acoustic field. Knowing the surface area $S$ of the boundary and the maximum frequency of interest, the required number of acoustic elements is given as $S/(\pi/3f_{max})^2$. Three matrices of this size will be required to compute the matrix multiplication, and it is usually best to do the computations in double-precision, thus requiring 16 bytes for each element of the matrices.

## Modeling sound—structure coupling

Recall that a moving structure compresses and contracts neighboring fluids, which act as a continuous elastic blob around the structure. When the fluid is heavy, its pressure loading affects the structural vibrations. To compute these effects, the boundary element model must be coupled to a representation of the structure.

The previous analysis has shown that an acoustic impedance matrix, relating the pressures to the normal component of velocity on the boundary surface, can be computed as a function of frequency using boundary element methods. We now want to combine this result with a finite element analysis of the structural vibrations to include the effects of the pressure field. In a finite element analysis, the displacements are written in the form

$$\left(-\omega^2\mathbf{M} - i\omega\mathbf{B} + \mathbf{K}\right)\mathbf{d} = \mathbf{F} \quad , \tag{29}$$

where **M**, **B**, and **K** are the mass, damping, and stiffness matrices, **d** is the displacement field of the structure, and **F** is the vector of forces applied to the structure.

To include the pressure field in the finite element analysis, the impedance matrix must be transformed from its dependence on normal surface velocity to nodal displacements. For time-harmonic problems, the displacement field on the outer surface of the structure can be used to compute the normal component of the surface velocity as a simple dot-product: $v_n = \mathbf{v} \cdot \mathbf{n} = -i\omega\, \mathbf{d} \cdot \mathbf{n}$. Thus, a matrix relationship can be derived to convert the complete displacement field into a normal surface velocity vector. This matrix will have zeros for all interior nodes not in contact with the surrounding fluid. Similarly, the matrix will also be zero for displacement degrees of freedom on the boundary surface tangential to the outward surface normal. Post-multiplying the acoustic impedance matrix by the transformation matrix then yields a matrix relationship between the pressure field on the boundary and the finite element displacement vector. Including the result for the pressure field on the boundary surface in the finite element equations of motion yields

$$\left(-\omega^2\mathbf{M} - i\omega\mathbf{B} + \mathbf{K} + \mathbf{A}\right)\mathbf{d} = \mathbf{F} \ . \tag{30}$$

Given an input force vector, it is theoretically possible to solve this equation for the displacement vector, which now includes fluid coupling. In a finite element analysis, the equation system is highly-banded because each element only interacts with other elements through the nodes. However, in a boundary element analysis, every node interacts with every other node, so that the acoustic impedance matrix is generally fully-populated. It then becomes very time-consuming to solve the matrix system in its present form. Various alternative strategies are possible where the matrices are subdivided into degrees of freedom with and without fluid coupling. It is also possible to treat the acoustic pressure field on the boundary surface as the primary variable.[21] Ultimately, many researchers instead reformulate the problem in terms of a modal frequency response analysis (which is the approach we use at Penn State). In a modal frequency response, the mass, damping, and stiffness matrices are pre- and post-multiplied by mode shapes, and the applied force vector is pre-multiplied by the mode shapes. The resulting system, which is usually much smaller in size than the system defined in physical coordinates, is solved to compute modal coefficients. The modal coefficients tell us how much each mode contributes to the overall response, and are multiplied by the mode shapes to compute that physical response.

Using the coupled FE/BE formulation, the time required to compute and store the acoustic impedance matrix as a function of frequency typically dominates the overall solution times. To speed up this part of the process, it is common to condense the structural displacement variables into a coarser set of acoustic variables. To illustrate, Fig. 17 shows two structural and acoustic meshes for a loudspeaker.

Since both the structural and acoustic fields require approximately six elements per wavelength, this process assumes that the structural waves vary more rapidly than the acoustic waves. This is true below the coincidence frequency, and is valid up to a relatively high frequency for structures submerged in water.

To demonstrate the typical results of a coupled FE/BE analysis, two example problems will be considered. The first is the familiar example of a thin circular cylindrical shell in

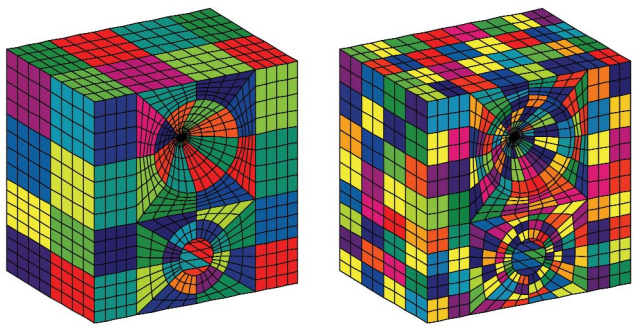

*Fig. 17. A structural mesh for a speaker with two different acoustic meshes.*

an infinite circular baffle. For simply-supported boundary conditions, the structural displacements can be determined analytically. Similarly, the acoustic Green's function is known analytically for a simple source outside of a rigid circular cylinder, and thus for this problem the acoustic field can also be determined analytically, although it can only be evaluated numerically. Solutions for the *in vacuo* and fluid-coupled resonance frequencies are given by Berot and Peseux.[23] For this problem, the cylinder has radius 0.4 m, length 1.2 m, and is 3 mm thick. Its material properties are given as E = 200 GPa, $\rho$ = 7850 kg/m$^3$, $\nu$ =0.3, and the surrounding water has properties $c_o$ = 1500 m/s, and $\rho_o$ = 1000 kg/m$^3$. We note that the thickness–to-radius ratio is less than 0.01 for this example, and thus thin shell theory is applicable and we expect a relatively large shift in the resonance frequencies due to fluid-loading. Our goal will be to reproduce Berot and Peseux's results. In the numerical computations, the structural analysis proceeds as usual, but we cannot simply model the boundary surface in the acoustic analysis because the circular baffle extends to infinity in both directions.

Following the procedure used by Berot and Peseux in their numerical computations, we will truncate the baffle on both sides of the cylinder approximately half its length beyond the vibrating portion and close off the ends with flat endcaps. Figure 18 shows the first two computed in vacuo mode shapes and resonance frequencies for the shell.

In the finite element analysis, the displacement is set to zero at the ends of the cylinder in the radial and torsional directions, but the axial displacement is unconstrained. As we will show, a fairly fine mesh is required in the circumferential direction to properly represent the acoustic impedance of the higher order modes. For example, to correctly represent a mode with 8 circumferential wavelengths, we need (8)(6)=48 acoustic elements around the circumference. The acoustic mesh does not have to be nearly as refined in the axial direction because the structural stiffness is much higher. With this in mind, the structural mesh has 24 elements in the axial direction and 48 elements around the circumference. The acoustic meshes have 8, 12, and 12 elements in the axial direction, and 16, 24, and 48 elements

| | | $\mathbf{f}_{\text{fluid}} / \mathbf{f}_{\textit{in vacuo}}$ | | | | | | |
|---|---|---|---|---|---|---|---|---|
| **Analysis Method** | **NA** | **(1,5)** | **(1,4)** | **(1,6)** | **(1,3)** | **(1,7)** | **(2,6)** | **(1,2)** |
| **Analytical** | - | 0.489 | 0.456 | 0.520 | 0.421 | 0.547 | 0.527 | 0.391 |
| **FE/BE** | 320 | 0.605 | 0.548 | 0.653 | 0.486 | 0.684 | 0.663 | 0.427 |
| | 720 | 0.545 | 0.498 | 0.589 | 0.448 | 0.629 | 0.601 | 0.401 |
| | 1440 | 0.491 | 0.455 | 0.523 | 0.418 | 0.553 | 0.538 | 0.382 |

*Table 2. Analytical and numerical predictions for the resonance frequency ratios (in fluid/in vacuo) of the circular shell. Mode orders are indicated as (m,n) pairs, where m is the order along the axis, and n is the circumferential harmonic.*

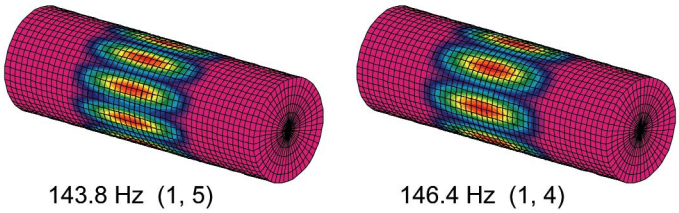


*Fig. 18. Finite element predictions for the first two mode shapes and resonance frequencies of a thin shell. The rigid ends on both sides of the shell simulate semi-infinite rigid baffles.*

around the circumference. Table 2 lists the resonance frequency ratios given by Berot and Peseux along with numerical predictions for the various acoustic element meshes.

In the table, **NA** is the number of acoustic elements for each of the boundary element meshes. Clearly, the numerical and analytical predictions match each other closely, although a relatively fine acoustic mesh is necessary in the circumferential direction to achieve convergence for the higher order modes, as was expected. Overall, for structures submerged in water, the fluid-loading analyses has been shown to yield excellent predictions for the added mass.

We consider a cavity-backed plate as a second example problem with structural-acoustic coupling. In the 1970's, Guy and Bhattacharya[24] studied transmission loss through a cavity-backed finite plate and their results have been used subsequently by several authors to validate numerical predictions. We will similarly use the problem to illustrate how dipole sources can be used to model interior and exterior acoustic fields simultaneously in a scattering problem. Figure 19 shows the geometry of the cavity and plate.

The plate is 0.914 mm thick and is made of brass with properties $E$ = 106 GPa, $\rho$ = 8500 kg/m$^3$, $\nu$ = 0.3, and the surrounding air has properties $c_o$ = 340 m/s, and $\rho_o$ = 1.2 kg/m$^3$. The plate is simply-supported and the backing cavity has rigid walls. We want to compute the transmission loss through the plate to a field point location at the center of the back wall of the cavity. Guy and Bhattacharya's transmission loss is actually just a ratio of the incident pressure and the pressure near the back wall of the box:

$$20\log_{10}(p_{interior} / p_{incident}) . \qquad (31)$$

For the numerical analysis, we can perform the computations in one of two ways. We could simply apply mechanical forces to produce a uniform pressure to the top surface of the plate, as in the studies by S. Suzuki, *et al.*[25] and M. Guerich and M. A. Hamdi,[26] or we could simulate the experiment using an acoustic source as the excitation. We will use the latter method. The surface of the cube is divided evenly into 144 quadrilateral elements, yielding a boundary surface mesh with 864 structural elements.

The incident pressure is computed knowing the source location and the distance to the center of the plate. The results in Fig. 20 show very good agreement between our numerical predictions and Guy and Bhattacharya's experi-

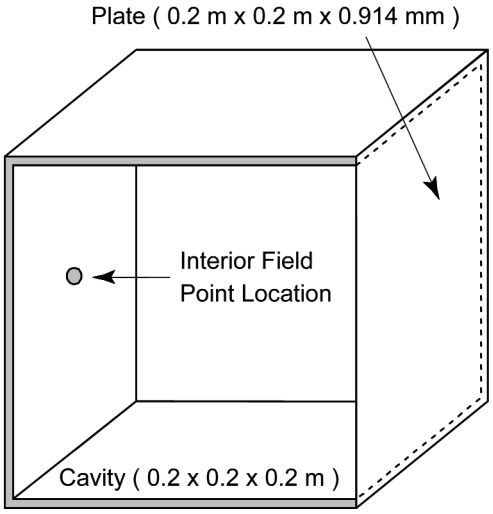


*Fig. 19. Dimensions for the cavity-backed plate example problem.*

mental measurements, thus demonstrating that dipole sources can be used to model both the interior and exterior acoustic fields simultaneously.

## Summary

In Part 2 of this tutorial on structural acoustics, we have learned about how acoustic fluids interact with structures, both as an acceptor and a cause of vibrational energy. We have presented some simple and difficult concepts in a relatively short article (entire textbooks are devoted to the subjects we have discussed), and hope the information is useful as a handy reference. For those of you who are interested in learning more about these topics, please look through the references we have provided. You are also welcome to enroll in the Sound—Structure Interaction course offered by the Penn State Graduate Program in Acoustics for a more thorough treatment of this subject.

Of course, there is much we have not explained, but we can refer you to other strong references on those subjects. For example, we have focused almost entirely on the interaction of structures with exterior fluids. Acoustic cavities contain resonances which can interact with the walls that bound the interior space, particularly at low frequencies. Some classic papers which introduce this topic are those by Pretlove[27] and Dowell.[28] During the Active Noise Control (ANC) boom of the 1980's and 1990's, many people investigated how to control the sound within acoustic cavity modes by driving the enclosure boundaries with tuned forces. Nelson and Elliott's textbook[29] is a good reference on ANC.

Another relatively modern structural–acoustic topic is Nearfield Acoustic Holography (NAH), which is an inverse technique for inferring a structure's surface vibrations from a complex pressure hologram measured near the surface. Once the surface velocities are known, numerical boundary value techniques can be used to compute the far-field sound radiation. We recommend the textbook by Williams[30] to those interested in NAH.

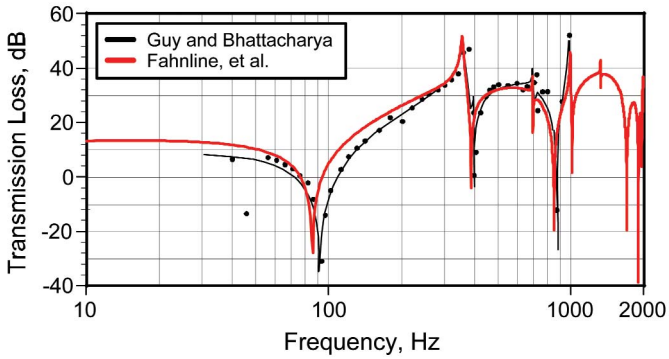


*Fig. 20. Transmission loss as a function of frequency for a cavity-backed plate.*

## Acknowledgments

We are grateful for our daily interaction with the ARL/Penn State Structural Acoustics Department (Andrew Barnard, Robert Campbell, Stephen Conlon, David Jenkins, and Tim McDevitt), along with some of our students in Penn State's Graduate Program in Acoustics, in particular, Ben Doty, who measured the response of the elbowed pipe. **AT**

## References for further reading

1 G. H. Koopmann and J. B. Fahnline, *Designing Quiet Structures* (Academic Press, San Diego, 1997).

2 R. D. Blevins, *Flow-Induced Vibration, 2nd Edition* (Krieger Publishing Company, Malbar, FL, 2001).

3 E. Naudascher and D. Rockwell, *Flow-Induced Vibrations–An Engineering Guide* (Dover Publications, Mineola, NY 2005).

[4] F. J. Fahy, *Sound and Structural Vibration: Radiation, Transmission, and Response* (Academic Press, San Diego, 1987).

[5] A. D. Pierce, *Acoustics–An Introduction to its Physical Principles and Applications* (Acoustical Society of America, Melville, NY, 1991).

[6] M. S. Junger and D. Feit, *Sound, Structures, and Their Interaction* (Acoustical Society of America, Melville, NY, 1993).

[7] G. Maidanik, "Response of Ribbed Panels to Reverberant Acoustic Fields," J. Acoust. Soc. Am. **34**, 809–826 (1962).

[8] C. E. Wallace, "Radiation Resistance of a Rectangular Panel," J. Acoust. Soc. Am. **51**, 946–952 (1972).

[9] P. W. Smith, Jr., "Response and Radiation of Structural Modes Excited by Sound," J. Acoust. Soc. Am. **34**, 640–647 (1962).

[10] C. B. Burroughs, R. W. Fischer, and F. R. Kern, "An Introduction to Statistical Energy Analysis," J. Acoust. Soc. Am. **101**, 1779–1789 (1997).

[11] P. J. Shorter and R. S. Langley, "On the Reciprocity Relationship Between Direct field Radiation and Diffuse Reverberant Loading," J. Acoust. Soc. Am. **117**, 85–95 (2005).

[12] M. J. Crocker and A. J. Price, "Sound Transmission Using Statistical Energy Analysis," J. Sound Vibration **9**, 469–486 (1969).

[13] A. J. Price and M. J. Crocker, "Sound Transmission Through Double Panels Using Statistical Energy Analysis," J. Acoust. Soc. Am. **47**, 683– 693 (1970).

[14] ISO 3741/ANSI S12.51, *Determination of Sound Power Levels of Noise Sources using Sound Pressure – Precision Methods for Reverberation Rooms* (Acoustical Society of America, Melville, NY, 1999).

[15] ISO 354, *Measurement of Sound Absorption in a Reverberation Room* (International Organization for Standardization, Geneva, 2003).

[16] S. C. Conlon, S. A. Hambric, and W. K. Bonness, "Evaluation of a reverberant water tank for radiated power measurements," *Proceedings of NoiseCon 2004*, Baltimore, MD, 12–14 July 2004. (Institute of Noise Control Engineering, Ames, IA, 2004).

[17] B. J. Doty, S. A. Hambric, S. C. Conlon, and J. B. Fahnline, "Structural-Acoustic Measurements of Pipes with Ninety-Degree Elbows, Under Water Loading," *Proceedings of NoiseCon 2005*, Minneapolis, MN, 17–19 October 2005 (Institute of Noise Control Engineering, Ames, IA, 2005).

[18] ANSI S12.35–1990 (R1996), *Determination of Sound Power Levels of Noise Sources in Anechoic and Hemi-Anechoic Rooms*, (Acoustical Society of America, Melville, NY, 1996).

[19] L. J. Gray and E. Lutz, "On the Treatment of Corners in the Boundary Element Method," J. Comp. Appl. Math. **32**, 369–386 (1990).

[20] L. G. Copley, "Integral Equation Method for Radiation from Vibrating Bodies," J. Acoust. Soc. Am. **41**, 807–816 (1967).

[21] H. A. Schenck, "Improved Integral Formulation for Acoustic Radiation Problems," J. Acoust. Soc. Am. **44**, 41–58 (1968).

[22] L. H. Chen and D. G. Schweikert, "Sound Radiation from an Arbitrary Body," J. Acoust. Soc. Am. **35**, 1626–1632 (1963).

[23] F. Berot and B. Peseux, "Vibro-acoustic behavior of submerged cylindrical shells: Analytical formulation and numerical model," J. Fluids and Struct. **12**(8), 959–1004 (1998).

[24] R. W. Guy and M. C. Bhattacharya,"The transmission of sound through a cavity-backed finite plate," J. Sound Vib. **27**(2), 207–223 (1973).

[25] S. Suzuki, S. Maruyama, and H. Ido, "Boundary element analysis of cavity noise problems with complicated boundary conditions," J. Sound and Vib. **130**(1), 79–91 (1989).

[26] M. Guerich and H. A. Hamdi, "A numerical method for vibro-acoustic problems with incompatible finite element meshes using B-spline functions," J. Acoust. Soc. Am. **105**(3), 1682–1694 (1999).

[27] A. J. Pretlove, "Forced Vibrations of a Rectangular Panel Backed by a Closed Rectangular Cavity," J. Sound Vib. **3**, 252–261 (1966).

[28] E. H. Dowell, G. F. Gorman, and D. A. Smith, "Acoustoelasticity: General Theory, Acoustic Natural Modes and Forced Response to Sinusoidal Excitation, Including Comparisons with Experiment," J. Sound Vib. **52**, 519–542 (1977).

[29] P. A. Nelson and S. J. Elliott, *Active Control of Sound* (Academic Press, San Diego, 1993).

[30] E. G. Williams, *Fourier Acoustics–Sound Radiation and Nearfield Acoustic Holography* (Academic Press, San Diego, 1999).

*Steve Hambric and his daughter Lily.*

Stephen A. Hambric is head of the Structural Acoustics Department at the Applied Research Lab at Penn State and Associate Professor in the Graduate Program in Acoustics. Prior to joining Penn State in 1996, Dr. Hambric worked for nine years in the Computational Mechanics Office at the Naval Surface Warfare Center, Carderock Division. Dr. Hambric has directed many numerical and experimental flow and structural acoustics research and development programs for the Navy, U.S. industry, and the U.S. Nuclear Regulatory Commission. He has authored over 60 conference and journal articles and advised many graduate students at Penn State. He teaches courses in Structural Acoustics, and Writing for Acousticians on campus at Penn State, and also to off-campus students working in industry and government. He currently serves on the board of directors of the Institute for Noise Control Engineering (INCE), on the Executive Committee of the ASME's Noise Control and Acoustics Division, and as an associate editor of ASME's Journal of Vibration and Acoustics.

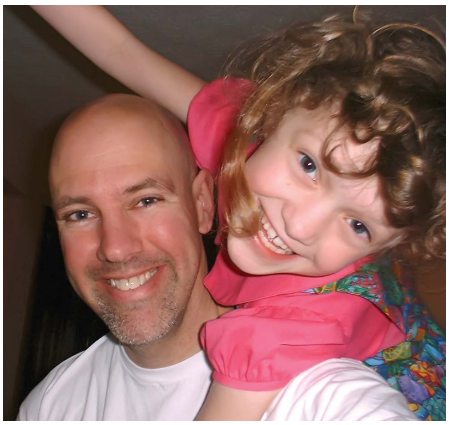

*John Fahnline (in background) and his niece Mariel.*

John B. Fahnline is a research associate at the Applied Research Laboratory and an assistant professor of acoustics at Penn State. He holds a Ph.D. in Acoustics from the Pennsylvania State University. As a post-doctoral researcher, Dr. Fahnline designed and implemented a practical, efficient, and accurate method for numerically solving general, three dimensional acoustic radiation problems which can be applied to problems in design optimization and active noise control. The code, named POWER, is currently being used at the ARL Penn State to predict noise radiation from the structural resonances of compound propulsors. Dr. Fahnline coauthored a book on design optimization with Dr. Gary Koopmann.